The use of Apatite II™ to remove divalent metal ions zinc(II), lead(II), manganese(II) and iron(II) from water in passive treatment systems: Column experiments

Josep Oliva [a], Joan De Pablo [b], José-Luis Cortina [b,c,*], Jordi Cama [d], Carlos Ayora [d]

[a] Department of Mining Engineering and Natural Resources, Universitat Politècnica de Catalunya, Bases de Manresa 61-73, 08242 Manresa, Catalonia, Spain
[b] Department of Chemical Engineering, Universitat Politècnica de Catalunya, Diagonal 647, 08028 Barcelona, Catalonia, Spain
[c] Water Technology Center, CETaqua, Paseo de los Tilos 3, 08034 Barcelona, Spain
[d] Institute of Environmental Assessment and Water Research, IDAEA, CSIC, Jordi Girona 18, 08034 Barcelona, Catalonia, Spain

ARTICLE INFO

ABSTRACT

The conventional passive treatments for remediation of acid mine drainage using calcite are not totally efficient in the removal of certain heavy metal ions. Although pH increases to 6–7 and promotes the precipitation of trivalent and some divalent metals as hydroxides and carbonates, the remaining concentrations of some divalent metals ions do not fulfill the environmental regulations. In this study, Apatite II™, a biogenic hydroxyapatite, is used as an alternative reactive material to remove Zn(II), Pb(II), Mn(II) and Fe(II). Apatite II™ reacted with acid water releasing phosphate and increasing pH up to 6.5–7, inducing metals to precipitate mainly as metal–phosphates: zinc precipitated as hopeite, $Zn_3(PO_4)_2 \cdot 4H_2O$, lead as pyromorfite, $Pb_5(PO_4)_3OH$, manganese as metaswitzerite, $Mn_3(PO_4)_2 \cdot 4H_2O$ and iron as vivianite, $Fe_3(PO_4)_2 \cdot 8H_2O$. Thus, metal concentrations from 30 to 75 mg L^{-1} in the inflowing water were depleted to values below 0.10 mg L^{-1}. Apatite II™ dissolution is sufficiently fast to treat flows as high as 50 m/a. For reactive grain size of 0.5–3 mm, the treatment system ends due to coating of the grains by precipitates, especially when iron and manganese are present in the solution.

© 2010 Elsevier B.V. All rights reserved.

1. Introduction

Water pollution produced by heavy metals in mining operations and mineral processing is a major environmental problem. Thus, in many mining areas with presence of poly metal-sulphides (Fe, Mn, Zn, Pb, Ni, Co, Cu), the release of these metals into groundwaters occurs, and non-admissible levels are found in surface and groundwaters. This has been translated in new regulatory requirements in most countries [1].

With the aim at remediate contaminated groundwater, pumping and ex situ treatments have been often employed. However, recent studies have shown that solubility constraints and low-permeability zones may prevent pumping from removing sufficient mass of contaminant to achieve the regulatory water quality standards. Additionally, the high economical cost associated makes this solution unrealistic in the case of acid mine drainage [2,3].

A potential solution to groundwater pollution by acid drainage problems is the installation of permeable reactive barriers (PRBs) into aquifers affected by drainage water derived from mine waste materials [4]. The PRB is a passive technique which implants a reactive material along the migration path of the polluted aquifer, where groundwater flows and reacts with the material from the barrier, so that, it neutralizes the acidity and retains metals. The PRB fill material is effective if [5]: it is enough reactive to reduce the concentrations of the pollutants; it is enough permeable to concentrate the groundwater flow through the barrier; it preserves the permeability and reactivity during a long period of time and, the filling material is available and cheap.

In passive systems to treat acid mine drainage (AMD), such as reducing and alkalinity producing system (RAPS) and PRB, organic matter with calcite is used as filling material [6,7]. Due to two main reasons they only remove part of the metal load from groundwater. First, sulphate reduction is a slow process and water needs a long residence time within the barrier for the reduction to take place [8]. This would require uneconomically thick barriers for the fluxes commonly found in alluvial aquifers. Second, due to the high Ca concentration in AMD, the pH values reach up to 6 and 7 due to calcite dissolution equilibrium. In previous studies [9], it was shown that although this pH allows precipitation of hydroxides of trivalent metals (Fe, Al, Cr), it is not high enough for divalent metal hydroxides to form (Zn, Mn, Cu, Pb, Ni, Co and Cd). The high pH

* Corresponding author at: Department of Chemical Engineering, Universitat Politècnica de Catalunya, Diagonal 647, 08028 Barcelona, Spain.
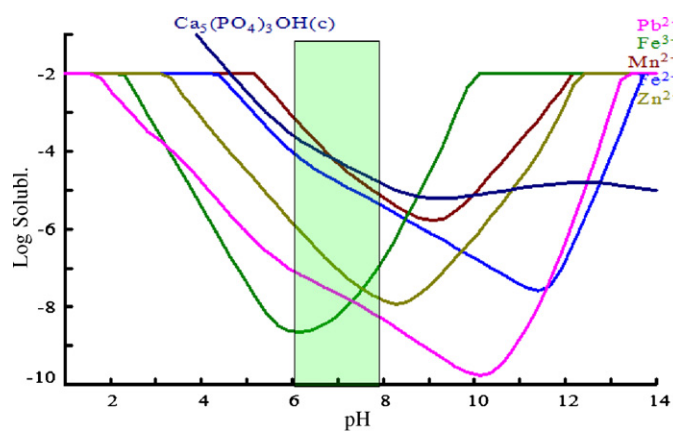*E-mail address:* jose.luis.cortina@upc.edu (J.-L. Cortina).

Fig. 1. Variation of metal concentrations in equilibrium with the metal–phosphates using the speciation code HYDRA and MINTEQ database [12]. In the absence of phosphate, the maximum concentration assumed is 0.01 mol L^{-1}. The amount of phosphate (PO$_4$$^{3-}$) in solution is that in equilibrium with apatite (dark blue line). The shaded rectangular field indicates the yielded pH range using hydroxyapatite as a passive treatment of acid water. (For interpretation of the references to color in this figure legend, the reader is referred to the web version of the article.)

values needed to remove most divalent metals from water can be reached by means of more basic reactive materials as magnesium oxide dissolution [10,11], or with a reactive material promoting the formation of more insoluble mineral phosphates. The solubility of metal–phosphates covers a very wide range in the low acidic to basic pH values (Fig. 1) that provides a higher removal capacity for divalent transition metals than carbonates or hydroxides [10].

An option as reactive material for PRBs is the use of hydroxyapatites. Hydroxyapatites have similar solubility as compared with other phosphates and promote the nucleation of metal–phosphate overcoming high activation energies. Moreover, they are stable, do not induce biological processes and they are good sorbents [13–15].

In the last years, both synthetic hydroxyapatite [13,16], mineral phosphate rocks [17–20] and biogenic hydroxyapatites [21–23] have been postulated as suitable material for both metal stabilization in soils and effluent treatment. Recently, a primarily low crystalline form of a carbonated hydroxyapatite of biogenic origin has been commercialized under the trade name of Apatite II^{TM}.

The use of Apatite II^{TM} to stabilize metal pollution in soils, under the approach identified as phosphate-induced metal stabilization (PIMS^{TM}) process has been reported [24,25]. Likewise, the use of Apatite II^{TM} in groundwater treatment applications is being under development [21,26,27]. Most of the published studies have only provided information on removal efficiency of metallic species, basically using batch experiments [13–20,26,28–30], and discussions have been mainly based on the use of sorption isotherms [14,15,26,27]. A few efforts have been made to identify the main physicochemical processes involved, specially the chemical reactions taking place and the identification of the mineral phases formed during the treatment steps [31]. Additionally, it should be mention that laboratory studies using flow-through column experiments are lacking. This type of experiments provide very valuable information on the physical aspects that affect the changes in porosity and permeability of the reactive media and also are very useful to determine the changes on the effluent composition due to the relative competition between the dissolution–precipitation rate and the water flux. However, the amount of solid precipitated in long flow-through experiments is larger than in batch experiments as allows the identification of the solid phases, and the recognition of the retention reactions.

The present paper investigates the Apatite II^{TM} removal capacity of Zn, Pb, Mn and Fe using column experiments emulating large-scale passive remediation systems. Apatite II^{TM} was defined as potentially suitable to remove Zn and Pb down to the very low regulatory concentrations for water fluxes expected in aquifers and infiltration ponds. Removal of common metals such as Fe and Mn, in the divalent form, with lower regulatory constraints has been also addressed, since both cations in the divalent form are poorly removed using the standard technologies of AMD. In addition, sulphate-rich waters to simulate AMD conditions have been used.

2. Experimental

2.1. Materials

The apatite used in this study is Apatite II^{TM} (US Patent #6,217,775), a biogenically precipitated apatite material that

Table 1
Initial conditions in the column experiments.

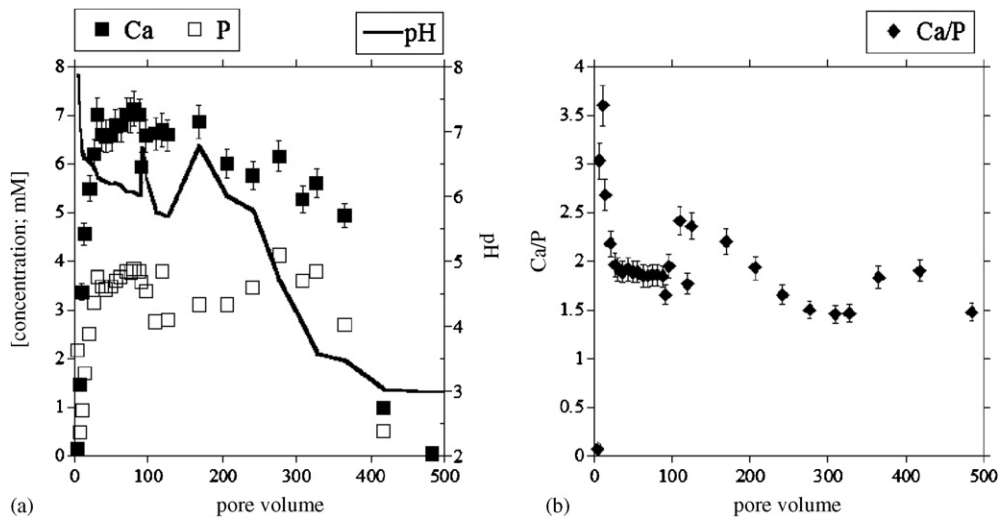|		Column experiments						
		0	1	2	3	4	5	6
Length	mm	17	44	44	41	36	17	16
Section	mm^2	172	172	172	172	172	172	172
Volume	mL	3	7.5	7.5	7	6.2	3.0	2.7
Sample	g-Initial	2.492	2.541	2.536	2.544	2.542	2.564	2.511
	g-Final	1.102	–	–	–	–	3.389	1.805
Particle size	mm	0.5–3	0.5–3	0.5–3	0.5–3	0.5–3	0.5–3	0.5–3
Apatite II^{TM}	wt.%	100	100	100	100	100	100	100
Pore volume	mL	1.5	5.9	5.9	5.4	4.6	1.4	1.2
Porosity		0.5	0.8	0.8	0.8	0.7	0.5	0.4
BET surface area	m^2/g-Initial	1.9	1.9	1.9	1.9	1.9	1.9	1.9
	m^2/g-Final	100	–	–	–	–	62	108
Flow rate	mL min^{-1}	0.02	0.02	0.02	0.02	0.02	0.02	0.02
Residence time	min	73	297	297	272	232	71	58
pH		4.5	3.0	3.1	5.6	5.6	4.6	4.0
Zn	mM		0.76		0.76			
Pb	mM			0.14		0.14		
Mn	mM						1.37	
Fe	mM							1.34
NO$_3$$^-$	mM					16.13		
SO$_4$$^{2-}$	mM	10.41			10.41		10.41	20.82

Fig. 2. Variation of pH and concentration of total Ca and P with pore volume in a representative experiment (a) and Ca/P molar ratio (b). pH of the inlet solution was 3 (H_2SO_4) and flow rate = 0.22 mL min^{-1}).
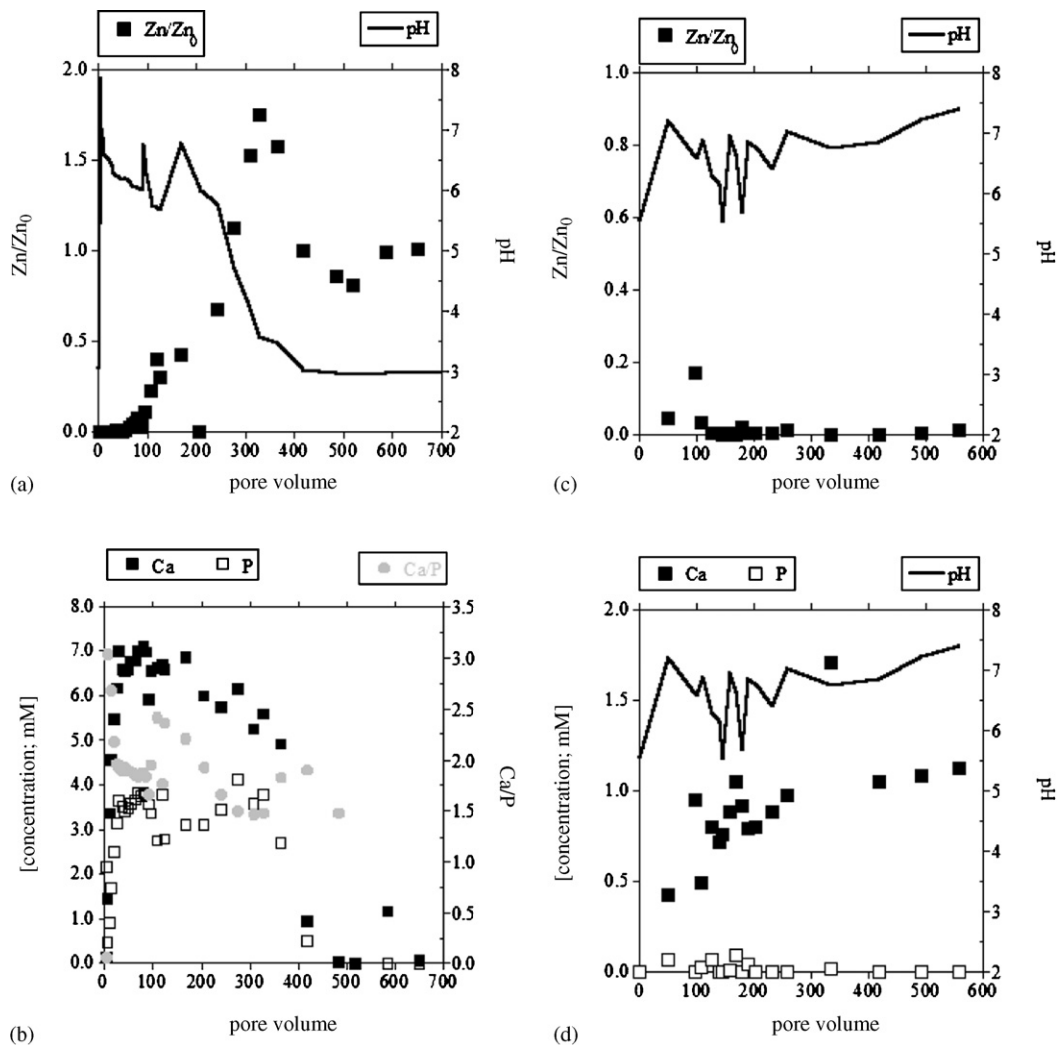

Fig. 3. Variation of (a) pH and [Zn/Zn$_0$] and (b) concentration of Ca and P and Ca/P ratio as a function of pore volume at initial pH 3. Variation of (c) pH, and [Zn/Zn$_0$] and (d) concentration of Ca and P as a function of pore volumes at initial pH 5.6. Zn$_0$ is initial concentration of Zn, 0.75 mM.
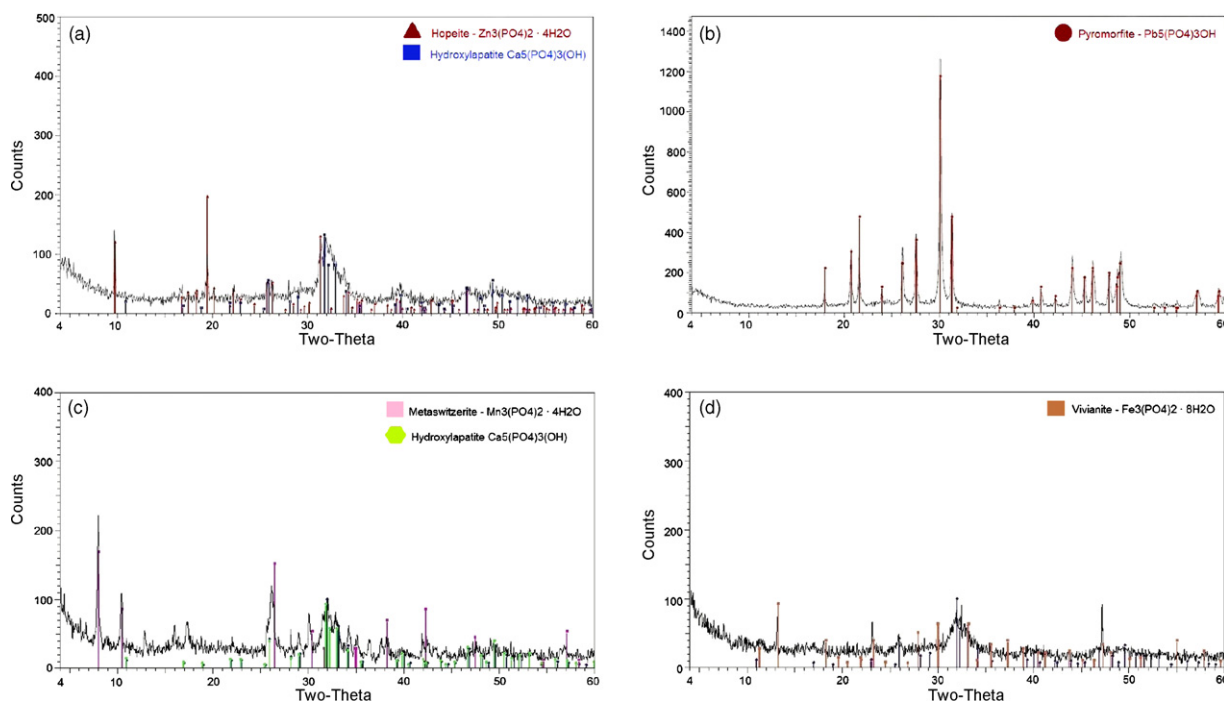
Fig. 4. X-ray diffraction patterns: (a) experiment with zinc, (b) experiment with Pb, (c) experiment with Mn and (d) experiment with Fe.

Table 2
Retention capacity of different hydroxyapatites.

Metal	Hydroxyapatite resource	pH initial	pH final	S^a [mg/g]	S^b [mg/g]	Reference
Zinc	Apatite II™	3.1	6.3	11.3	–	Column experiment (1)[c]
	Apatite II™	3.1	3.0	15.5	–	Column experiment (1)[d]
	Apatite II™	5.6	7.4	>59	–	Column experiment (3)
	Apatite II™	6.4	6.6	8.3	8.52	[26]
	Apatite II™	–	–	50.0	–	[25]
	Mineral	1–12	>6.5	41.0	–	[20]
	Mineral	5.5	–	–	1.17–6.33	[33]
	Mineral	2.0–6.0	–	–	8.54	[34]
	Synthetic	6.7	5.4	0.98–47.4	76.51	[32]
	Synthetic	6.0	–	7.2–51.6	–	[30]
	Synthetic	3.0–12.0	–	22.0	37.50	[35]
	Synthetic	5.9–6.6	5.6–7.2	9.7–37.1	37.14	[37]
	Bone char	4.8	5.0	~37	35.2	[38]
	Activated mineral	2.0–6.0	–	–	12.26	[34]
Lead	Apatite II™	3.1	4.1	22.1	–	Column experiment (2)[c]
	Apatite II™	3.1	2.9	33.6	–	Column experiment (2)[d]
	Apatite II™	5.6	7.6	>35	–	Column experiment (4)
	Apatite II™	5.4	7.0	20.2	–	[26]
	Apatite II™	–	–	200.0	–	[24]
	Mineral	5.5	–	–	19.4–34.0	[33]
	Mineral	1–12	3–10.5	151.0	–	[20]
	Mineral	2.0–6.0	–	–	12.78	[34]
	Synthetic	3.0–5.0	4.0–5.5	300–450	330–450	[19]
	Synthetic	3.0–12.0	–	79.6	676.1	[35]
	Synthetic	–	–	230.0	–	[16]
	Synthetic	2.0–9.0	4.0–8.5	~145	145.0	[36]
	Activated mineral	2.0–6.0	–	–	15.47	[34]
	From gypsum waste	2.0–9.0	3.0–9.5	~500	500.0	[36]
	From poultry waste	2.0–9.0	3.5–11	~250	227.0	[36]
Manganese	Apatite II™	4.5	8.2	18.5	–	Column experiment (5)[c]
	Apatite II™	4.5	6.5	126.0	–	Column experiment (5)[d]
	Apatite II™	7.1	6.5	9.0	–	[26]
	Apatite II™	–	–	50.0	–	[25]
Iron	Apatite II™	4.0	6.9	57.1	–	Column experiment (6)[c]
	Apatite II™	4.0	5.1	124.2	–	Column experiment (6)[d]
	Apatite II™	6.6	6.2	11.3	–	[26]
	Apatite II™	–	–	50.0	–	[25]

[a] Capacity of retention in mg of metal for g of retention material.
[b] Maximum sorption capacity by isotherm in mg of metal for g of retention material.
[c] Capacity of retention in time of break in the experiment.
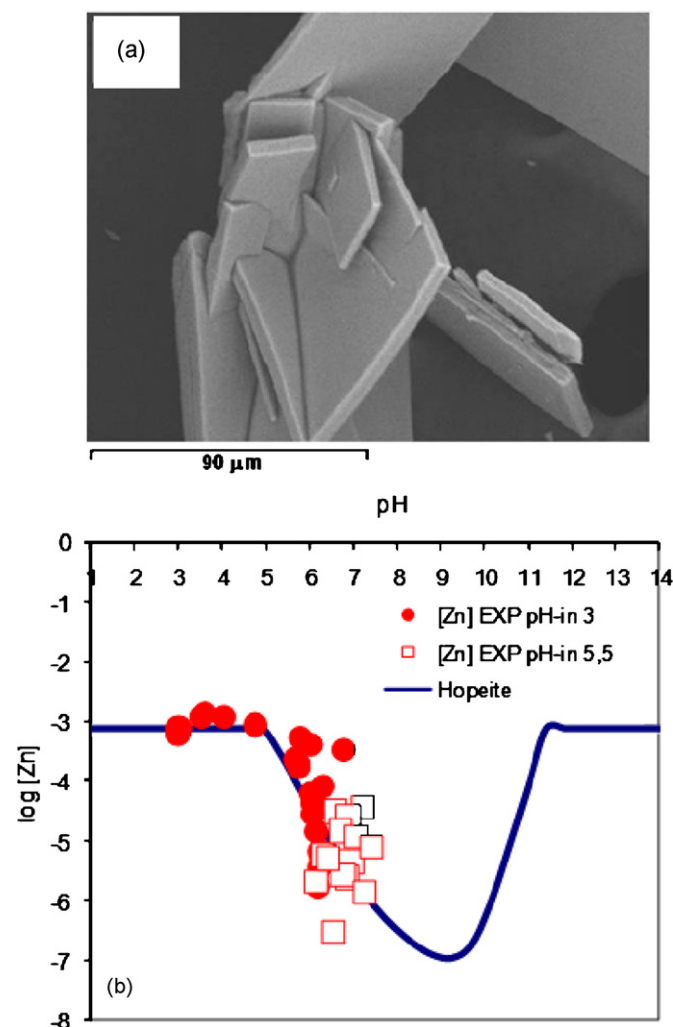[d] Top value in the experiment.

Fig. 5. SEM image of an aggregate of tabular crystals of hopeite ($Zn_3(PO_4)_2 \cdot 4H_2O$) (a). Variation of Zn(II) concentration with pH of the outlet solutions. Plotted metal concentrations in equilibrium with the phosphorus solid phases were calculated using the speciation code HYDRA [12] (b).

is derived from fish bones and has the general composition $Ca_{10-x}Na_x(PO_4)_{6-x}(CO_3)_x(OH)_2$, where $x < 1$, along with 30–40% by weight of associated organic materials in the internal porosity of the inorganic structure [27]. XRD patterns show that the raw material consists mainly of hydroxyapatite with calcite content of up to 5 wt.%. The grain size of the used samples ranges from 0.5 to 3 mm. The initial BET surface area is $1.9 \pm 0.2 \, m^2/g$. The final BET surface area was measured in most of the experiments and ranged from 62 to $108 \, m^2/g$ (Table 1).

2.2. Methods

Column experiments were designed to measure the reactivity of Apatite II^{TM} under flow conditions, similar to the one expected in transmissive aquifers. Solutions were administered continuously through Teflon tubing connected to a Gilson Minipuls® peristaltic pump. The inlet fluxes employed are shown in Table 1. Tracer tests were conducted by adding a known concentration of acetone to the saturating solution to verify uniformity of flow in the columns and to determine the effective porosity. The out flowing solutions were introduced into a Hewlet-Packard HP53® spectrophotometer by using a follow-through cuvette for continuous monitoring of acetone. Measured pore volumes for the different columns are given in Table 1.
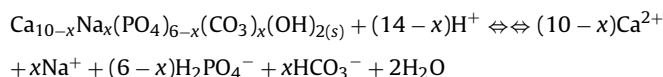
Inflowing solutions were prepared either with the metal sulphate salt or with the metal nitrate salt and ultrapure Mili-Q water. In three experiments the sulphate concentration was 10.4 and 20.82 mM (1000 and 2000 mg L^{-1}) by adding sodium sulphate (reagent grade, Merck). One experiment contained 16.1 mM (1000 mg L^{-1}) of nitrate by adding sodium nitrate (reagent grade, Merck) (Table 1). pH of the inflowing solutions ranged from 3.05 to 5.56 (Table 1). Initial concentrations of Zn, Pb, Mn and Fe ranged between 0.14 and 1.37 mM (30 and 75 mg L^{-1}) (Table 1). pH was measured in sealed flow-through cells placed at the exit of the columns. Effluent solutions were filtered through 0.45 μm filter and acidified with HNO$_3$ to pH < 1. Cation concentrations were measured by inductively coupled plasma (ICP-AES). The accuracy of the measurements was around 3%. Flow rates were determined gravimetrically.

At the end of the column experiments, the reacted material was examined by SEM–EDS a JEOL 3400® scanning electron microscopy with energy dispersive system. Crystal phases in the final column fillings were identified with a BRUKER D5005® X-ray diffractometer (XRD), with Cu Lα radiation.

3. Results and discussion

3.1. Dissolution experiments

Dissolution of Apatite II^{TM} provided detectable concentrations of Ca and P. In general, the concentration of Ca and P and pH increased initially with time (Fig. 2a), and steady state was achieved after approximately 2 h and remained during 75 pore volumes. A measured Ca/P molar ratio of about 1.7 was attributed to be the stoichiometric Ca/P molar ratio of the raw sample (Fig. 2b). Output pH values of the reacting solution were between 6 and 8. Since, according to the stoichiometric formula, the phosphate content is higher than that of carbonate ($0 < x < 1$), the phosphate system ($H_2PO_4^-/HPO_4^{2-}$) was considered as responsible for buffering pH:

$$Ca_{10-x}Na_x(PO_4)_{6-x}(CO_3)_x(OH)_{2(s)} + (14-x)H^+ \Leftrightarrow\Leftrightarrow (10-x)Ca^{2+}$$

$$+ xNa^+ + (6-x)H_2PO_4^- + xHCO_3^- + 2H_2O$$

Thus, Apatite II^{TM} dissolution provides strong pH buffering capacity. Additionally, Apatite II^{TM} dissolution supplied constantly $H_2PO_4^-$ anions, which would be used to precipitate metal–phosphates.

The dynamic conditions in the columns showed the strong capacity of Apatite II^{TM} to neutralize high acidic waters (e.g., from initial pH values of 3 to 5) with high flow rates (up to 0.5 m d^{-1}). While Apatite II^{TM} was available and dominant over the experiments, outflow pH ranged between 5 and 6.5, and concentrations of calcium and total phosphorous were higher than 3 mM (Fig. 2a). After 350 pore volumes the amount of Apatite II^{TM} was practically consumed: effluent pH was the same than the influent one, and concentration of phosphorous and calcium was below detection limit.

3.2. Zinc removal

Two solutions that contained 0.76 mM (50 mg L^{-1}) of Zn at pH 3 in a sulphate-free solution and pH 5.6 in a sulphate-rich solution (Table 1, experiments 1 and 3) were used to study the removal of zinc. The experiments lasted for 5 and 3 months, respectively. Variation of concentrations of P, Ca and Zn and reacting pH as a function of pore volume (PV) is shown in Fig. 3. Phreeqc calculations show that the solution was undersaturated with respect to calcite (saturation index < −3) at the first pore volumes of the experiment. Fast dissolution of calcite at this stage raised the
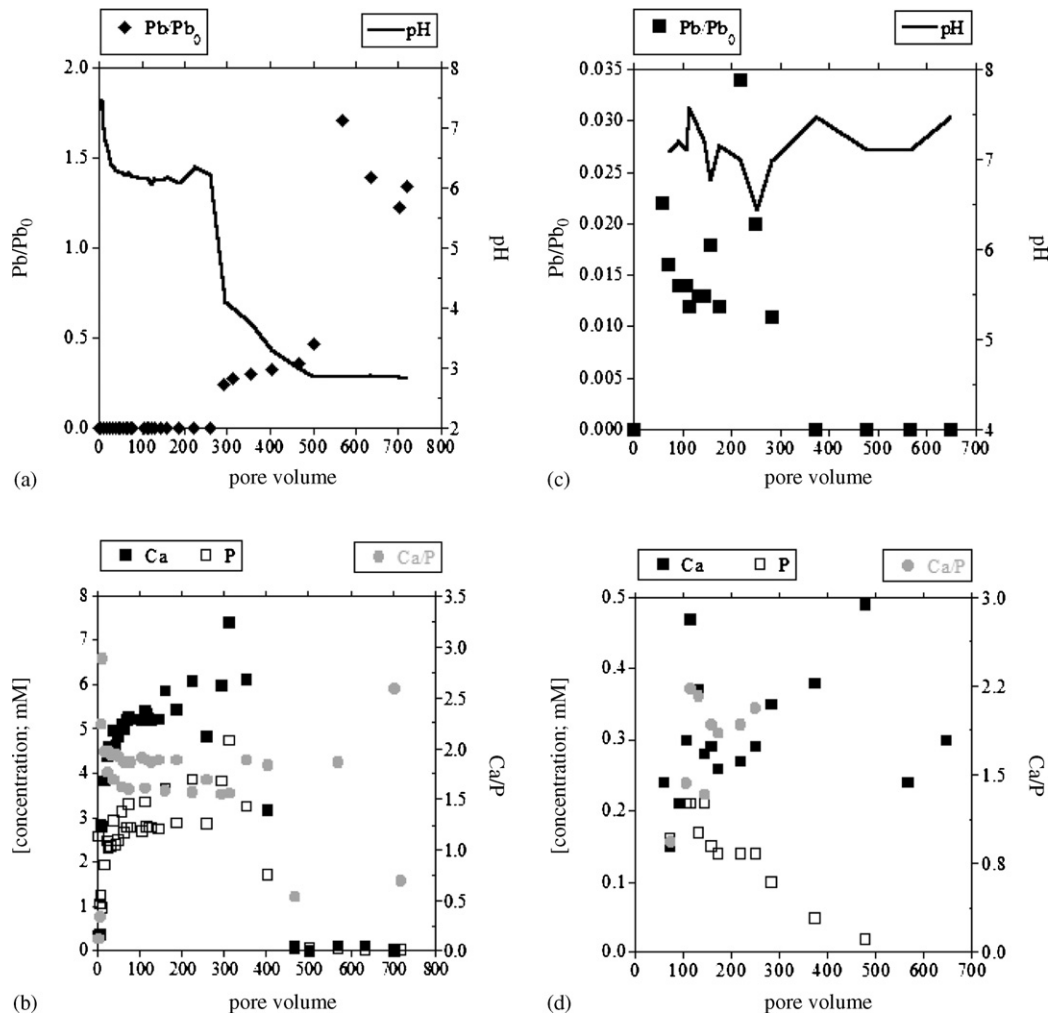
Fig. 6. Variation of (a) pH and [Pb]/[Pb$_0$] and (b) Ca and P of the outlet solution and Ca/P ratio in the experiment with input pH of 3.1. Evolution of (c) pH and [Pb]/[Pb$_0$] and (d) Ca and P of the outlet solution and Ca/P ratio in the experiment with input pH of 5.6. Pb$_0$ is initial concentration of Pb, 0.14 mM.

solution pH to 7–7.5. Thereafter, calcite was consumed and pH decreased to 6–7, indicating Apatite II^{TM} control. In the experiment with an input pH of 3, an outflow pH of 6.2 lasted for more than 200 pore volumes, while Zn was efficiently removed from solution with total concentration of Zn below 0.3 mM (Fig. 3a). The molar ratio of Ca/P of the outlet was higher than 1.7 (the stoichiometric Ca/P molar ratio of Apatite II^{TM}) due to deficit of aqueous phosphorous, which was consumed by zinc phosphate precipitation.

Between 250 and 400 pore volumes, pH dropped to 3 (input pH) along with decrease of concentration of Ca and P, and The Ca/P ratio showed some variability mostly between 1.5 and 2.5 (Fig. 3b). Mass balance calculations indicate that more than 45 wt.% of initial Apatite II^{TM} was consumed. Thus, pH fall is associated to decrease of the neutralizing agent mostly due to the armouring of Apatite II^{TM} surface with precipitates, or to the switch from pervasive pore to preferential flow paths caused by precipitates. In either case, the amount of reactive material used was higher than the used limestone [9] or magnesium oxide [10,11] in passive treatments. As pH decreased to 3, a significant increase in zinc content was observed (up to 1.34 mM or 80 mg L^{-1}) for more than 20–40 pore volumes, exceeding the inflowing value of 0.76 mM. This fact is originated by dissolution of the newly formed Zn-phosphates. Hence, a remediation system based on the reactions described above must be renewed when symptoms of exhaustion

appear. Both the extraction of the exhausted reactive material in the treatment and the use of extractable containers could be possible approaches.

The experiment with higher inflow pH (5.6) resulted in an outflowing pH value over 7 in the whole experimental run (more than 600 pore volumes). Zn content was efficiently removed from solution (below 0.05 mM) (Fig. 3c). A pH increase as Apatite II^{TM} dissolved was related to an increase in total Ca (up to 1.1 mM) (Fig. 3d). Concentration of P was below 0.1 mM as released phosphate by Apatite II^{TM} dissolution was consumed in the precipitation of zinc phosphate (Fig. 3d). A mass balance calculation indicates that only 87 wt.% of the starting hydroxyapatite was consumed after 600 pore volumes.

XRD patterns of the reacted material revealed the presence of hopeite (Zn$_3$(PO$_4$)$_2$4H$_2$O) (Fig. 4a). SEM–EDS examination of the precipitates confirmed the presence of Zn–P–O-bearing solids. Tabular to prismatic crystals, occurring as divergent aggregates of hopeite were observed (Fig. 5a). Aqueous Zn concentration is in accordance with that expected from an equilibrated solution with respect to hopeite as shown in Fig. 5b. Hopeite has been described in soil stabilization, as well as in treatment of aqueous solutions containing zinc [21,22]. Lee et al. [31], evaluating the mechanisms of Zn–hydroxyapatite interaction, observed that precipitation of hopeite dominated the removal of Zn(II) when its concentration was higher than 1 mM (64 mg L^{-1} Zn(II)). However, sorption of Zn

onto hydroxyapatite was also suggested as the dominant process in low ranges of Zn(II) concentration where no precipitates formed [26].

3.3. Lead removal

Two nitrate-rich solutions containing 0.145 mM (30 mg L^{-1}) of Pb at pH 3.1 and 5.6 were used as inflow solutions (Table 1, experiments 2 and 4). Sulphate-rich solutions were discarded to prevent precipitation of lead sulphate. The experiments lasted for 5 and 3 months at pH 3.1 and pH 5.6, respectively. Variation of concentration of P, Ca and Pb and pH as a function of pore volume is depicted in Fig. 6.

Similar to the Zn experiments, initial dissolution of calcite, increased pH values to 7.5–8. After calcite consumption, pH decreased to 6–7, indicating Apatite II^{TM} dissolution. In the experiment at pH 3.1, outflow pH of 6–6.5 was observed for more than 250 pore volumes (Fig. 6a). At this stage, Pb was efficiently removed from solution, yielding lead concentrations below 0.00015 mM. In this period the Ca/P molar ratio is higher than 1.7 (the stoichiometric Ca/P molar ratio of Apatite II^{TM}) due to deficit of aqueous phosphorous, which was consumed by lead–phosphate precipitation.

After 450 pore volumes, pH dropped to input pH of 3 along with decrease of concentration of Ca and P (Fig. 6b). Mass balance shows that more than 60 wt.% of initial Apatite II^{TM} was consumed. Hence, pH fall is associated with loss of Apatite II^{TM} reactivity, since its reactive surface diminished due to surface passivation by lead-precipitate formation. As pH decreased below 3, a remarkable increase in aqueous lead concentration was observed, exceeding the inflowing value (0.176 mM) and reaching 0.24 mM (50 mg L^{-1}) for more than 20 pore volumes (Pb/Pb$_0$ > 1 in Fig. 6a). As in the case of zinc, this excess of aqueous lead is attributed to dissolution of newly precipitated Pb-bearing solids.

In the experiment at pH 5.6, the outflow pH ranged was between 6.5 and 7.5 over the experimental run (700 pore volumes), being Pb efficiently removed from solution ([Pb] < 0.021 mM) (Fig. 5c). pH increased as Apatite II^{TM} dissolved and is associated with the increase of total Ca (up to 0.5 mM) (Fig. 6d). Concentration of P was below 0.22 mM due to the fact that phosphate released during Apatite II^{TM} dissolution was uptaken by lead–phosphate precipitation, yielding a deficit in aqueous phosphorous (i.e., Ca/P molar ratio > stoichiometric Ca/P molar ratio). Mass balance calculation yielded 40 wt.% of consumed hydroxyapatite.

XRD patterns of the retrieved materials showed the presence of pyromorphite (Pb$_5$(PO$_4$)$_3$OH) as a major Pb phase (Fig. 4b). The SEM–EDS examination confirmed the presence of Pb–P–O-bearing solids. Pyromorphite formed clusters of hexagonal prisms (Fig. 7a). Aqueous Pb(II), PO$_4$$^{3-}$ and H$^+$ concentration in the outlet solution was in accordance with that expected from equilibrium with respect to pyromorphite (Fig. 7b). Pyromorphite formation occurs in batch and column experiments of soil stabilization and treatment of containing lead solutions using apatite [15,17,20,28]. These studies showed that the process of Pb(II) removal or uptake by hydroxyapatite involves the dissolution of hydroxyapatite and precipitation of lead hydroxyphosphate, being pyromorphite the most common solid found. Recently, Mavropoulos et al. [28] reported formation of solid solution of Ca and Pb (Pb$_{(10-x)}$Ca$_x$ (PO$_4$)$_6$(OH)$_2$). With time a hydroxypyromorphite stoichiometry ratio of Pb/Ca equal to 1.67 is achieved. Based on the combination of XRD and chemical analyses, these authors showed that Pb(II) was not totally consumed by the formation of Pb$_{(10-x)}$Ca$_x$ (PO$_4$)$_6$(OH)$_2$. Part of this uptake (20–30%) was attributed to surface mechanisms such as sorption and complexation.
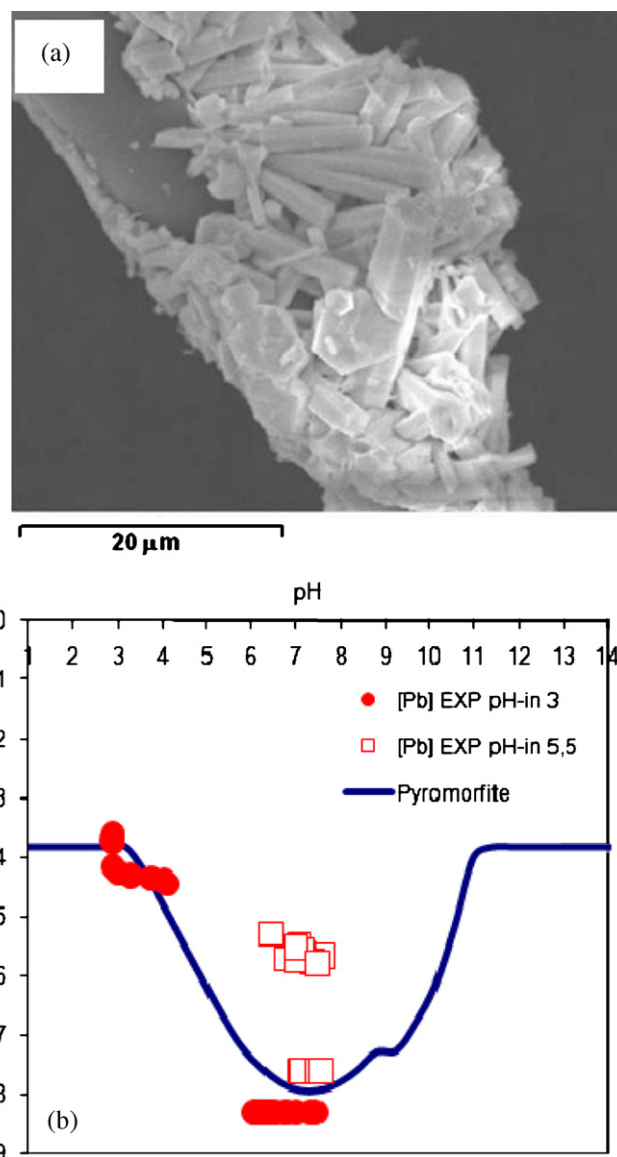

Fig. 7. SEM image that shows clusters of roselike aggregates of pyromorfite (Pb$_5$(PO$_4$)$_3$OH) on top of apatite surface (background) (a). Variation of Pb(II) concentration with pH in the outlet solutions. Plotted metal concentrations in equilibrium with the phosphorus solid phases were calculated using the speciation code HYDRA [12] (b).

3.4. Iron and manganese removal

Two sulphate-rich solutions with pH 4.0 and 4.6 and 1.34 mM Fe and 1.37 mM Mn (75 mg L^{-1}of Fe and Mn, respectively), were used as inflow solutions (Table 1, experiments 5 and 6). The experiments lasted for 11 and 17 months for Fe and Mn, respectively. Variation of concentration of Mn, Fe, P and Ca and pH as a function of pore volume is shown in Figs. 8 and 9.

In both experiments, the initial pH was higher than 8. This is due to fast dissolution of calcite as the reacting solution was undersaturated with respect to this carbonate. After calcite exhaustion, Ca concentration and pH dropped gradually as available Apatite II^{TM} dissolved (Figs. 8a and 9a). Released phosphate was uptaken by metal precipitation, and Mn and Fe were efficiently removed from solution up to 2000 pore volumes (Figs. 8b and 9b).

XRD patterns of the retrieved material from the manganese column revealed the presence of metaswitzerite (Mn$_3$(PO$_4$)$_2$4H$_2$O)) as the major Mn phase (Fig. 4c). SEM–EDS examination confirmed
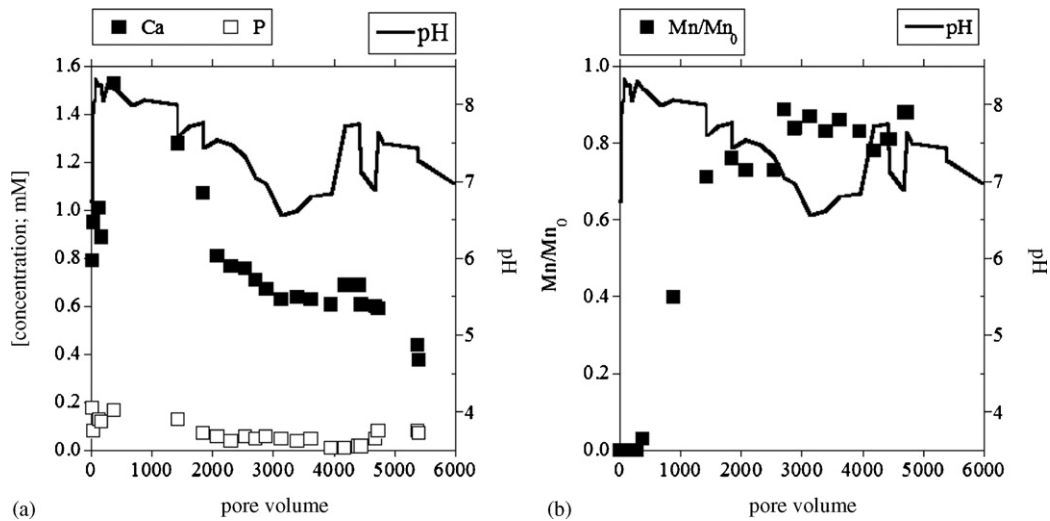
Fig. 8. Variation of (a) pH and concentration of Ca and P and (b) [Mn/Mn$_0$] as a function of pore volume (Mn$_0$ is initial concentration of Mn, 1.37 mM).

the presence of Mn–P–O-bearing precipitates. The observed amorphous and crystalline aggregates of thin flakes of metaswitzerite grew onto the surface of Apatite II^{TM} grains (Fig. 10a). Moreover, element mapping showed a surrounding layer covering the external part of the grain to be rich in Mn–P–O, whereas an internal region was rich in Ca–P–O (Fig. 10b–f). Furthermore, some zones formed by precipitates among grains, were highly rich in oxygen.

Solubility data of (Mn$_3$(PO$_4$)$_2$) is used to evaluate the variation of the measured concentration of Mn with pH (Fig. 11). At low pH, measured concentrations of Mn are concordant with the calculated ones. However at pH around 8 the dramatic decrease in Mn concentration suggests that another solid phase was formed.

Mn removal from AMD water is a very interesting case. The concentration of Mn(II) in equilibrium with respect to Mn(II) hydroxides is high at any pH [10,12]. Likewise, it was demonstrated that Mn(II) oxidized to Mn(III) at pH > 9 when a basic material (e.g., caustic magnesia) was used to remove aqueous Mn [10]. In the present study, the measured pH was close to 8 and low Mn(II) concentrations were measured. Therefore, possible partial oxidation of Mn(II) to Mn(III) and Mn(IV) and precipitation of manganese at different oxidation state as oxides and hydroxides could not be totally

ruled out. However, none of these hydroxide phases was detected by XRD.

Regarding iron removal, XRD patterns showed that vivianite (Fe$_3$(PO$_4$)$_2$8H$_2$O) was the major, newly precipitated Fe(II) phase (Fig. 4d). SEM–EDS examination of the precipitates shows the ubiquitous presence of clusters of Fe–P–O-bearing platty rhombic crystals of vivianite (Fig. 12a). The measured Fe concentrations agree with the calculated ones in an equilibrated solution with respect to vivianite (Fig. 12b). The stability of this phase spans over the pH range observed in the column.

Scarce data on Fe(II) and Fe(III) removal using hydroxyapatites can be found in the literature. Ma et al. [17] reported data on the use of hydroxyapatite for removal of heavy metals (Pb(II), Zn(II), Cu(II), Cd(II), Fe(II) and Al(III)) in batch experiments. The characterization of the hydroxyapatite material after the removal assays showed the formation of pyromorphite and hopeite in the experiments with Pb(II) and Zn(II), respectively. However, in Fe(II) removal experiments, these authors only observed some retention of Fe(II) on new phases but no Fe(II) solids were detected by XRD. Gschwend and Reynolds [29] reported on in situ subsurface formation of colloidal Fe phosphate solids, which were attributed to the interaction of different phosphate
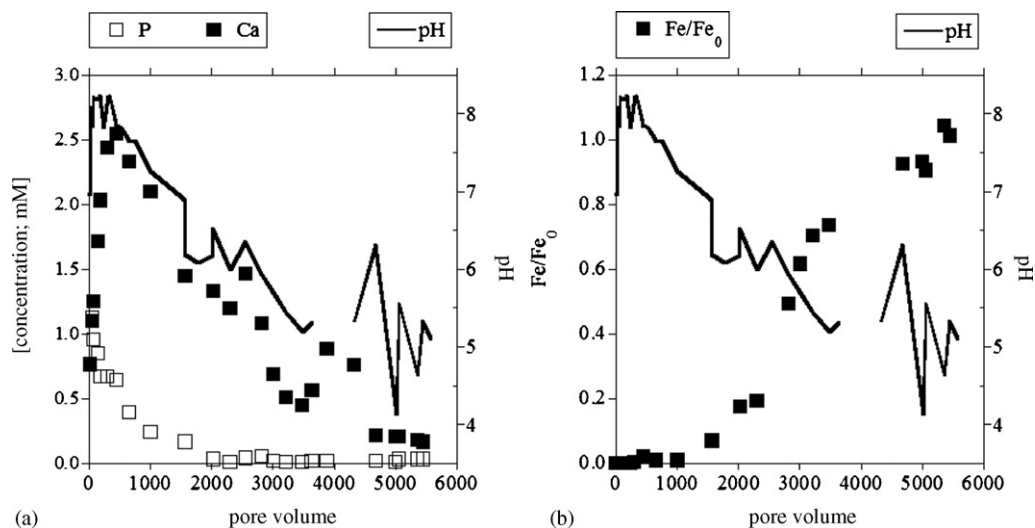

Fig. 9. Variation of (a) pH, and concentration of Ca and P and (b) [Fe/Fe$_0$] as a function of pore volume (Fe$_0$ is initial concentration of Fe, 1.34 mM).
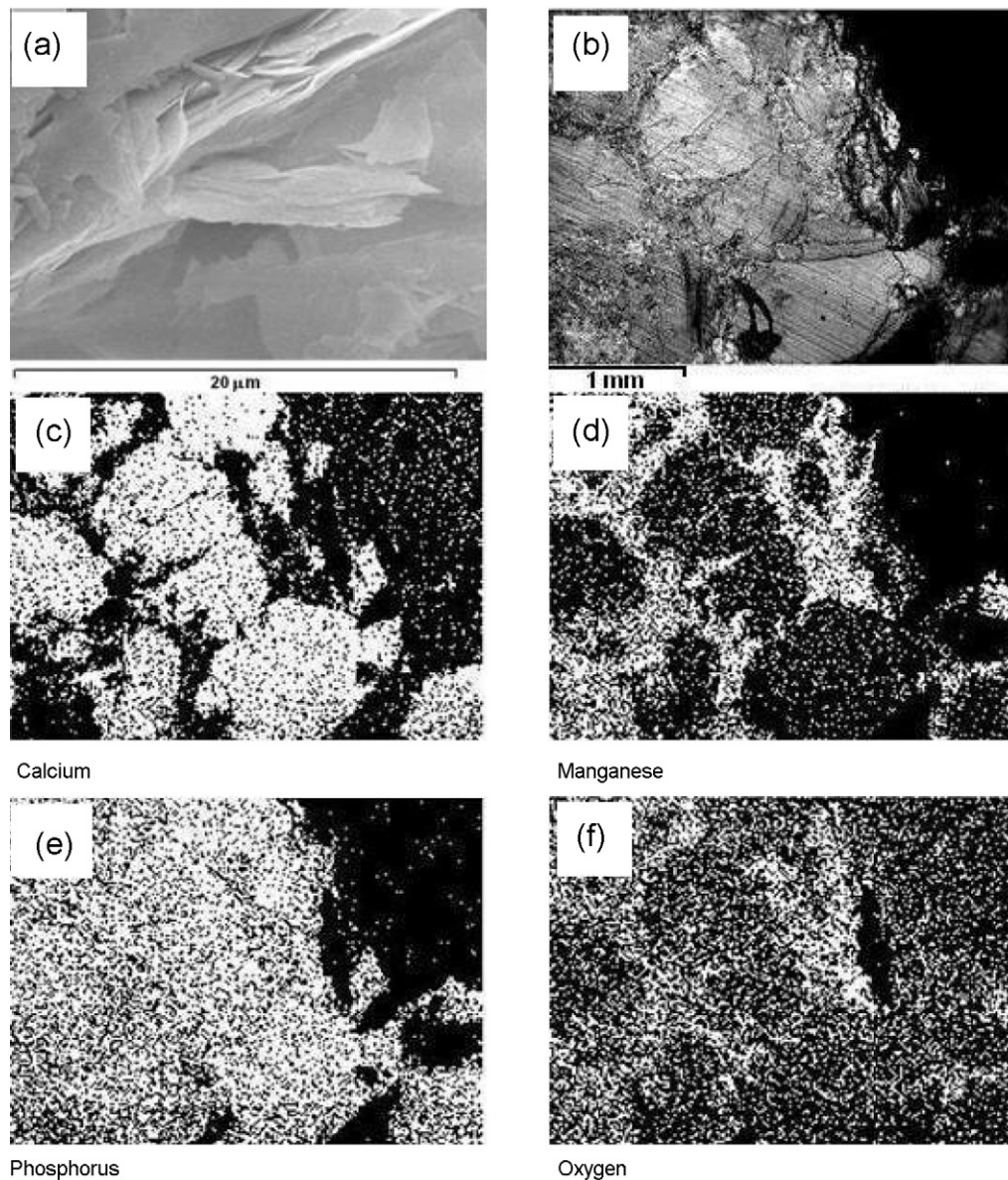
Fig. 10. SEM image of aggregates of metaswitzerite ($Mn_3(PO_4)_2 \cdot 4H_2O$) on top of the apatite surface (a). SEM image of the section of precipitate (b). Element mapping showing the element distribution on the sample (c–f).

species than combined with Fe(II) released from the solids of the aquifer. It was suggested that the colloidal solids were vivianite.

It should be noticed that under the yielded experimental conditions, other removal mechanisms could be expected. In the case of Fe(II), although the experiment was maintained in anoxic conditions, oxidation of Fe(II) to Fe(III) could be expected at pH > 5, promoting precipitation of Fe(III)-hydroxides (e.g., ferrihydrite). Although this process took place, these precipitates were not detected by XRD and SEM–EDS. Formation of ferrihydrite could account for the measured total iron concentrations of the effluent.

Likewise, in the case of Mn, at pH around 8 oxidation of Mn(II) to Mn(III) and Mn(IV) could occur and yield formation of Mn-oxides/hydroxides, providing values of Mn concentration closer to the measured ones and the predicted Mn concentrations in equilibrium with respect to metaswitzerite $Mn_3(PO_4)_2 4H_2O$. However, if these processes happened, examination by SEM–EDS and XRD analyses did not reveal their presence. Hence, although removal of Mn(II) and Fe(II) could be a mixture of two mechanisms (formation

of metal–phosphates and formation of metal-oxide/hydroxides), only the former has been clearly observed in this study.

4. Conclusions: use of Apatite II™ in passive treatments

Column experiments were carried out to study the removal of metals (Zn, Pb, Mn and Fe(II)) at acid pH range (3–5.6). At pH < 4 the removal capacity of zinc and lead before reaching the break-through point (assuming 10% of the input concentration, $C/C_o = 0.1$) is about 97%. This yields 11 mg zinc/g (5.8 mg/m^2) after 96 pore volumes and 22 mg lead/g (11.6 mg/m^2) after 293 pore volumes for lead. Similar removal capacity is observed at pH > 5. Before reaching the breakthrough point removal efficiencies of 98% of Zn (59 mg zinc/g (31 mg/m^2)) and 99% of lead (35 mg lead/g (18.4 mg/m^2)) were obtained. Hence, total consumption of Apatite II™ would be obtained after 2200 pore volumes.

Table 2 shows retention of zinc and lead per gram of Apatite II™ compared with hydroxyapatites of non-biogenic origin and synthetic calcium phosphates. The efficiency of Apatite II™ increases
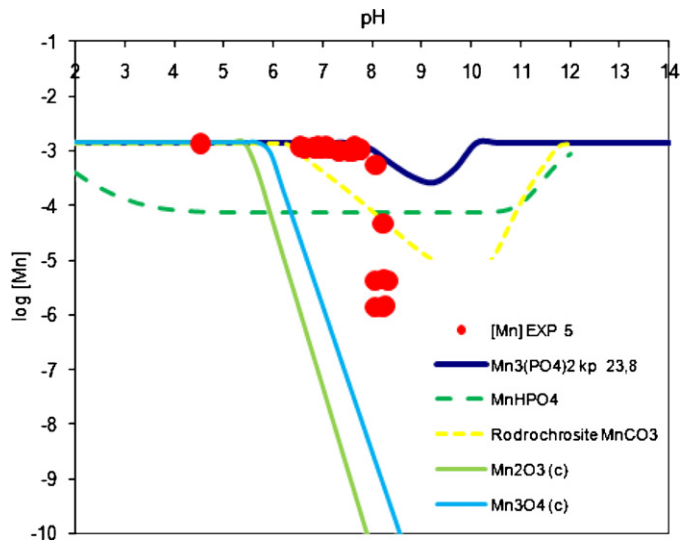
Fig. 11. Variation of measured Mn(II) concentrations with pH and metal concentration in equilibrium with other Mn phases using the MINTEQ database [12].

by decreasing water acidity. It stems that application of apatite-based materials for metal removal treatments should be restricted to slightly acid to neutral pH waste water. Under these conditions, consumption of reactive material to neutralize acidity is not the main mechanism taking place. The governing process is the use of phosphate ions, provided by apatite dissolution, to form metal–phosphate minerals.

Upscaling of these results to field scale treatment suggests that a barrier 1-m thick could be operative from 5 to 10 years with water flux as high as 1–10 $m^3/m^2/y$ if the treated-water pH is above pH 4. These results have been clearly shown in the experiments with Pb(II) and Zn(II) in the treated solution at pH between 4 and 5, where the experiments were stopped without reaching the breakthrough point. At lower pH (3–4) a high amount of hydroxyapatite dissolved, probably more than the needed to precipitate metal cations in solution.

Regarding to Fe(II) and Mn(II), Apatite II[TM] exhaustion occurred later, above 5500 pore volumes (340 days), although the column breakthrough was after 440 and 1500 pore volumes with Mn and Fe, respectively. Manganese removal efficiency was higher than 96% before the breakthrough with a removal capacity of 126 mg/g (66 mg/m^2) at the end of the experiment, yielding a global retention of 32%. The iron removal efficiency was 98%, the maximum capacity was 124.2 mg/g (66 mg/m^2), and the yielded retention was 46% (Table 2).

In contrast to the Zn and Pb experiments, at the end of the Fe and Mn experiments, some phosphate remained, being capable to neutralize the inflow acidity. As a consequence, at the resulting pH re-dissolution of newly precipitated metal–phosphates did not occur. The mass balance calculation showed that only 40 wt.% of Apatite II[TM] was consumed. The pH drop could be caused by armouring of Apatite II[TM] surface by precipitates or to a switch from pervasive pore to preferential flow paths caused by precipitates.

For the different column experiments carried out in the present study, clogging problems were hardly found. In comparison with other reactive materials such as limestone and caustic magnesia, where column operation is suffering of clogging due to porosity reduction by formation of precipitates, Apatite II[TM] showed more reliable behavior in hydraulic terms. Capacity of Apatite II[TM] to retain zinc, lead, iron and manganese from AMD at the common range of flow rates in aquifers, even up to 50 $m^3/m^2/y$, is remarkable.
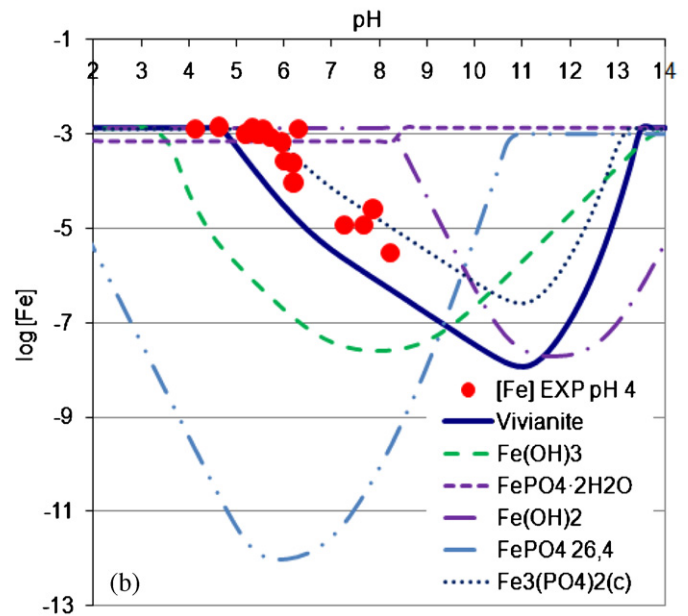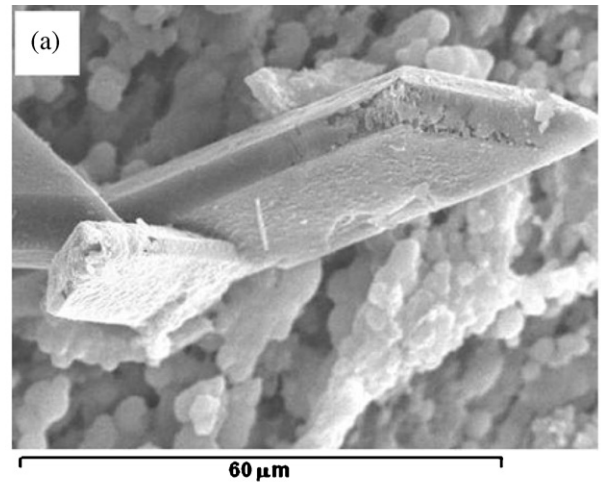

Fig. 12. SEM image of vivianite ($Fe_2(PO_4)_3 \cdot 8H_2O$) (a). Variation of Fe(II) concentration with pH of the outlet solutions. Plotted metal concentrations in equilibrium with the phosphorus solid phases were calculated using the speciation code HYDRA [12] (b).

Extrapolation of the laboratory-column durability of Apatite II[TM] to 1 m thick treatment of AMD suggests that Apatite II[TM] is active for 5–10 years if pH is higher than 4. This result encourages further studies to address the efficiency of apatite–base systems for treating highly acid waters (pH < 4), contemplating the use of mixtures with other materials (e.g. limestone) to remove acidity (H^{+}) and extend Apatite II[TM] duration.

Acknowledgements

References

[1] P.L. Younger, S.A. Banwart, R.S. Hedin, Minewater: Hydrology Pollution and Remediation, 1st ed., Kluwer Academic Publishers, Dordrecht, The Netherlands, 2002.

[2] PEREBAR, 5th Framework Programme Research and Technology Development Project on Long-term Performance of Permeable Reactive Barriers Used for the Remediation of Contaminated Groundwater, PEREBAR EVK1-CT-1999-00035, National Technical University of Athens, Greece, 2002.

[3] ITRC, Permeable Reactive Barriers: Lessons Learned/New Directions. Technical/Regulatory Guidelines, ITRC, Washington, DC, 2005.

[4] S.G. Benner, D.W. Blowes, W.D. Gould, R.B. Herbert, C.J. Ptacek, Geochemistry of a permeable reactive barrier for metals and acid mine drainage, Environ. Sci. Technol. 33 (1999) 2793–2799.

[5] D.W. Blowes, C.J. Ptacek, J.L. Jambor, In-situ remediation of Cr(IV)-contaminated groundwater using permeable reactive walls: laboratory studies, Environ. Sci. Technol. 31 (1997) 3348–3357.

[6] K.L. Ford, Passive treatment systems for acid mine drainage, Technical Note 409, BLM/ST/ST-02/001+3596, Bureau of Land Management, National Science & Technology Center, Denver, 2003, webbased report available online at http://www.blm.gov/nstc/library/techno2.htm.

[7] K.R. Waybrant, D.W. Blowes, C.J. Ptacek, Selection of reactive mixtures for use in permeable reactive walls for treatment of mine drainage, Environ. Sci. Technol. 32 (1998) 1972–1979.

[8] O. Gibert, J. de Pablo, J.L. Cortina, C. Ayora, Chemical characterisation of natural organic substrates for biological mitigation of acid mine drainage, Water Res. 38 (2004) 4186–4196.

[9] O. Gibert, J. de Pablo, J.L. Cortina, C. Ayora, Municipal compost-based mixture for acid mine drainage bioremediation: metal retention mechanisms, Appl. Geochem. 20 (2005) 1648–1657.

[10] J.L. Cortina, I. Lagreca, J. de Pablo, J. Cama, C. Ayora, Passive in situ remediation of metal-polluted water with caustic magnesia: evidence from column experiments, Environ. Sci. Technol. 37 (2003) 1971–1977.

[11] T.S. Rötting, J. Cama, C. Ayora, J.L. Cortina, J. de Pablo, Use of caustic magnesia to remove cadmium, nickel and cobalt from water in passive treatment systems: column experiments, Environ. Sci. Technol. 40 (2006) 6438–6443.

[12] I. Puigdomènech, Chemical Equilibrium Software Hydra and Medusa, Inorganic Chemistry Department, Technology Institute, Stockholm, Sweden, 2001.

[13] T. Suzuki, T. Hatsushira, Y. Hayakawa, Synthetic hydroxyapatites employed as inorganic cation-exchangers, J. Chem. Soc. Faraday Trans. I 77 (1981) 1059–1062.

[14] Q.Y. Ma, S.J. Traina, T.J. Logan, J.A. Ryan, Effects of aqueous Al, Cd, Cu, Fe(II), Ni and Zn on Pb immobilization by hydroxyapatite, Environ. Sci. Technol. 28 (1994) 1219–1228.

[15] X. Chen, J.V. Wright, J.L. Conca, L.M. Peurrung, Evaluation of heavy metal remediation using mineral apatite, Water Air Soil Pollut. 98 (1997) 57–78.

[16] T. Suzuki, T. Hatsushira, M. Miyake, Synthetic hydroxyapatites as inorganic cation-exchangers. Part 2, J. Chem. Soc. Faraday Trans. I 78 (1982) 3605–3611.

[17] Q.Y. Ma, T.J. Logan, S.J. Traina, Lead immobilization from aqueous solutions and contaminated soils using phosphate rocks, Environ. Sci. Technol. 29 (1995) 1118–1126.

[18] S. Raicevic, T. Kaludjerovic-Radoicic, A.I. Zouboulis, In situ stabilization of toxic metals in polluted soils using phosphates: theoretical prediction and experimental verification, J. Hazard. Mater. B117 (2005) 41–53.

[19] S. Baillez, A. Nzihou, D. Bernache-Assolant, E. Champion, P. Sharrock, Removal of aqueous lead ions by hydroxyapatites: equilibria and kinetic processes, J. Hazard. Mater. A139 (2007) 443–446.

[20] X. Chen, J.V. Wright, J.L. Conca, L.M. Peurrung, Effects of pH on heavy metal sorption on mineral apatite, Environ. Sci. Technol. 31 (1997) 624–631.

[21] J.L. Conca, J.V. Wright, Using an Apatite II PRB to remediate ground water contaminated with zinc, lead, and cadmium, The Remediation Technologies Development Forum Permeable Reactive Barriers Action Team Meeting, Best Western Winrock Inn Albuquerque, New Mexico, 2004.

[22] J. Wright, K.R. Rice, B. Murphy, J.L. Conca, PIMS-remediation of Pb-contaminated soil at camp Stanley, Texas, in: R.E. Hinchee, B. Alleman (Eds.), Sustainable Range Management, Battelle Press, Columbus, OH, 2004.

[23] S. Raicevic, J.V. Wright, V. Veljkovic, J.L. Conca, Theoretical stability assessment of uranyl phosphates and apatites: selection of amendments for in situ remediation of uranium, Sci. Total Environ. 355 (2006) 13–24.

[24] J.L. Conca, N. Lu, G. Parker, B. Moore, A. Adams, J.V. Wright, P. Heller, PIMS–remediation of metal contaminated waters and soils, in: G.B. Wickramanayake, A.R. Gavaskar, S.C. Chen (Eds.), Remediation of Chlorinated and Recalcitrant Compounds, vol. 6, Battelle Press, Columbus, Ohio, 2000, pp. 319–326.

[25] J. Wright, K.R. Rice, B. Murphy, J.L. Conca, PIMS using Apatite II™: how it works to remediate soil and water, in: R.E. Hinchee, B. Alleman (Eds.), Sustainable Range Management, Battelle Press, Columbus, OH, 2004.

[26] W.D. Bostick, Use of apatite for chemical stabilization of subsurface contaminants, Final Report, Work performed under contract: DE-AC26-01NT41306, US Department of Energy, 2003.

[27] J.L. Conca, J. Wright, An Apatite II permeable reactive barrier to remediate groungwater containing Zn, Pb and Cd, Appl. Geochem. 21 (2006) 2188–2200.

[28] E. Mavropoulos, A. Malta Rossi, A.M. Costa, C.A. Perez, J.C. Moreira, M. Saldanha, Studies on the mechanisms of lead immobilization by hydroxyapatite, Environ. Sci. Technol. 36 (2002) 1625–1629.

[29] P.M. Gschwend, M.D. Reynolds, Monodisperse ferrous phosphate colloids in an anoxic groundwater plume, J. Contam. Hydrol. 1 (1987) 309–327.

[30] M. Peld, K. Tonsuaadu, V. Bender, Sorption and desorption of Cd^{2+} and Zn^{2+} ions in apatite-aqueous systems, Environ. Sci. Technol. 38 (2004) 5626–5631.

[31] Y.J. Lee, E.J. Elzinga, R.J. Reeder, Sorption mechanisms of zinc on hydroxyapatite: systematic uptake studies and EXAFS spectroscopy analysis, Environ. Sci. Technol. 39 (2005) 4042–4048.

[32] A. Corami, S. Mignardi, V. Ferrini, Copper and zinc decontamination from single- and binary-metal solutions using hydroxyapatite, J. Hazard. Mater. 146 (2007) 164–170.

[33] X. Cao, L.Q. Ma, D. Rhue, C.S. Appel, Mechanisms of lead, copper and zinc retention by phosphate rock, Environ. Pollut. 131 (2004) 435–444.

[34] Z. Elouear, J. Bouzid, N. Boujelben, M. Feki, F. Jamoussi, A. Montiel, Heavy metal removal from aqueous solutions by activated phosphate rock, J. Hazard. Mater. 156 (2008) 412–420.

[35] I. Smiciklas, A. Onjia, S. Raicevic, D. Janackovic, M. Mitric, Factors influencing the removal of divalent cations by hydroxyapatite, J. Hazard. Mater. 152 (2008) 876–884.

[36] Y. Hashimoto, T. Sato, Removal of aqueous lead by poorly-crystalline hydroxyapatite, Chemosphere 69 (2007) 1775–1782.

[37] Y. Xu, F.W. Schwartz, S.J. Traina, Sorption of Zn^{2+} and Cd^{2+} on hydroxyapatite surfaces, Environ. Sci. Technol. 28 (1994) 1472–1480.

[38] C.W. Cheung, C.K. Chan, J.F. Porter, G. Mckay, Combined diffusion model for the sorption of cadmium, copper, and zinc ions onto bone char, Environ. Sci. Technol. 35 (2001) 1511–1522.